AIP | Applied Physics Letters

Highly efficient electron vortex beams generated by nanofabricated phase holograms

Vincenzo Grillo, Gian Carlo Gazzadi, Ebrahim Karimi, Erfan Mafakheri, Robert W. Boyd, and Stefano Frabboni

Citation: Applied Physics Letters **104**, 043109 (2014); doi: 10.1063/1.4863564
View online: http://dx.doi.org/10.1063/1.4863564
View Table of Contents: http://scitation.aip.org/content/aip/journal/apl/104/4?ver=pdfcov
Published by the AIP Publishing

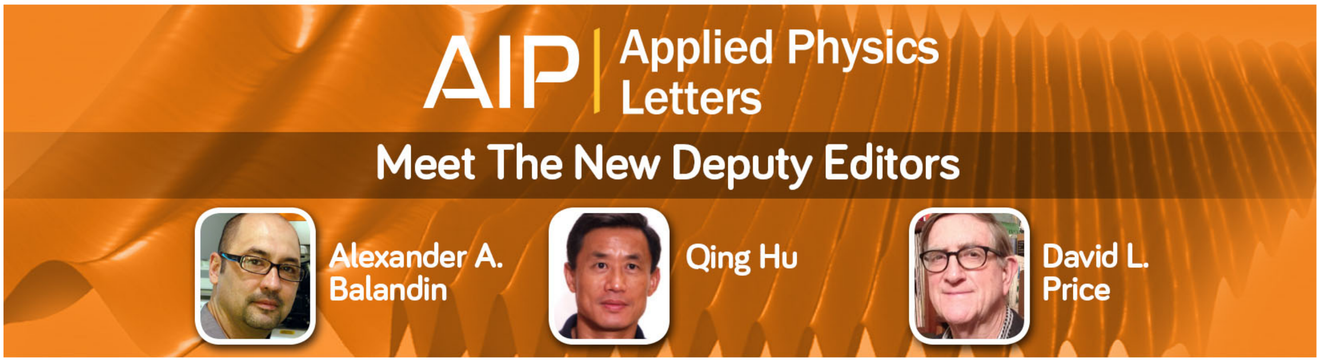

APPLIED PHYSICS LETTERS **104**, 043109 (2014)

Highly efficient electron vortex beams generated by nanofabricated phase holograms

Vincenzo Grillo,[1,2,a)] Gian Carlo Gazzadi,[1] Ebrahim Karimi,[1,3] Erfan Mafakheri,[4]
Robert W. Boyd,[3] and Stefano Frabboni[1,4]
[1]*CNR-Istituto Nanoscienze, Centro S3, Via G Campi 213/a, I-41125 Modena, Italy*
[2]*CNR-IMEM Parco Area delle Scienze 37/A, I-43124 Parma, Italy*
[3]*Department of Physics, University of Ottawa, 150 Louis Pasteur, Ottawa, Ontario K1N 6N5, Canada*
[4]*Dipartimento di Fisica Informatica e Matematica, Università di Modena e Reggio Emilia, via G Campi 213/a, I-41125 Modena, Italy*

(Received 13 November 2013; accepted 11 January 2014; published online 30 January 2014)

We propose an improved type of holographic-plate suitable for the shaping of electron beams. The plate is fabricated by a focused ion beam on a silicon nitride membrane and introduces a controllable phase shift to the electron wavefunction. We adopted the optimal blazed-profile design for the phase hologram, which results in the generation of highly efficient (25%) electron vortex beams. This approach paves the route towards applications in nano-scale imaging and materials science. © *2014 AIP Publishing LLC*. [http://dx.doi.org/10.1063/1.4863564]

Electron vortex beams were introduced a few years ago theoretically by Bliokh *et al.*[1] and subsequently observed experimentally by Uchida and Tonomura,[2] Verbeeck *et al.*,[3] and McMorran *et al.*[4] Vortex beams are characterized by a staircase-like wavefront and therefore by a phase singularity that is stable upon free propagation.[5]

These beams are creating a very large interest for both fundamental studies, since they are a discrete state and eigenstates of the orbital angular momentum (OAM),[6] and for application as promising tools for transmission electron microscopy (TEM),[7] among which the most remarkable is magnetic dichroism.[8] On the other hand, these beams have also been used to convey angular momentum to nanoparticles[9,10] and are predicted to be an essential element for the design of an electron spin polarizer.[11]

Unlike more conventional e-beam configurations, the realization of vortex beams is difficult with a conventional set of electromagnetic lenses.[12] In fact, so far the vortex beams have been realized mainly by the diffraction through holographic plates with a suitable pattern, having the shape of a pitch fork hologram.

The design of such holograms is typically quite simple: they consist of a binary mask that transmits only part of the wavefront. As a consequence, there is inevitably a net loss of intensity. The realization of these beams follows a holographic three steps process.[3,4] The first step involves the design of a computer-generated hologram produced by the interference of the vortex beam of topological charge ℓ that is $\Psi_{vortex}(r) = f(r)e^{i\ell\theta}$ (here the r and θ are the transverse polar coordinates and the phase term along the propagation direction is omitted) with a tilted reference plane wave: $\Psi_{ref} = e^{ik_\perp r_\perp}$(here $k_\perp$ and $r_\perp$ are the transverse wave vector component and spatial coordinate, respectively) thus giving $I_{hol} = |\Psi_{ref} + \Psi_{vortex}|^2$. The interference fringes forming the hologram are characterized by a carrier spatial frequency and are modulated in both intensity and spacing by the amplitude and phase of Ψ_{vortex}, having the characteristic *fork* shape. This pattern is, in turn, transformed into a digital mask I_{bin} with a threshold method. The second step is the realization of the physical hologram by transferring I_{bin} to a substrate, typically by milling through a membrane with focused ion beam (FIB). The last step is the insertion of the *holographic plate*, into the electron microscope.

The beam diffracted into the m-th order acquires a singular phase with topological charge $q = m\cdot\ell$. We will concentrate here on the case $\ell = 1$.

For an electron in the TEM, the wavelength is typically of picometer size (in our case, $\lambda = 2.51$ pm) and the holographic plate acts as a *diffraction grating* characterized by the transmittance

$$T_H(r_\perp) = A(r_\perp)e^{i\Delta\varphi(r_\perp)}, \tag{1}$$

where $A(r_\perp)$ and $\Delta\varphi(r_\perp)$ are the amplitude and phase modulations of the transmitted wave measured with respect to the incident plane wave. The electron vortex beam is then reconstructed in the diffracted beams, originating from the hologram when illuminated by an electron plane wave. Depending on the modulation imposed by the hologram on the incident wave, it is possible to classify the holograms as: (i) mixed hologram, modulated in both $A(r_\perp)$, $\Delta\varphi(r_\perp)$;[13] (ii) amplitude holograms, modulated in $A(r_\perp)$, $\Delta\varphi(r_\perp) = const$,[14] and (iii) phase holograms, modulated in $\Delta\varphi(r_\perp)$, $A(r_\perp) = const$.[15]

Physically, the amplitude modulation for transmitted electrons is mainly given by a combination of inelastic scattering and high-angle elastic scattering that removes electrons from the forward trajectory and is more important for heavy materials or thick samples. Conversely, the appropriate phase for transmitted electron is obtained as an effect of the mean inner potential of the material, V_{mip},[16] that produces a local acceleration of the wavefront over a region defined by the local hologram thickness.

The phase variation due to such potential is written as

$$\Delta\varphi(\bar{r}) = C_E\int_0^{t(r_\perp)} V_{mip}dz = C_E V_{mip}t(r_\perp), \tag{2}$$

[a)] Electronic mail: vincenzo.grillo@nano.cnr.it here $C_E = 7.5\,10^{-3}\,\frac{rad}{Vnm}$, for electrons of 200 keV energy, $t(r_\perp)$ is the local thickness of the sample. Since V_{mip} in most materials is of the order of 10–20 V, the difference in the optical path due to some 100 nm thick material is of the order of the wavelength.

Therefore, by changing the material, we can switch between a pure phase effect for light materials to a complete amplitude effect when heavy materials are introduced into the hologram. In the present work, we use a thin membrane (200 nm-thick) of amorphous Si_3N_4 as nearly pure phase object.

The prediction and control of the beam characteristics, in addition to high intensity, are crucial elements for all applications of electron vortex beams to materials science and should be optimized in the design stage of the hologram.

In Table I, we report a selection of groove profiles for both amplitude and phase holograms and the corresponding maximum diffraction efficiencies η_m defined as: $\eta_m = \frac{I_m}{I_{in}}$ (I_m being the intensity of the m-th beam and I_{in} being the intensity of the beam before the holographic plate) at one of the two first-order diffracted beams.

As can be deduced from Table I, the idea behind the use of phase holograms is to take advantage of the additional degree of freedom represented by the thickness profile to tune the amplitudes of the different diffracted beams. In this way, for example, the amplitude of the undiffracted beam (zero order) can be reduced virtually to 0.

It is worth noting the case of a "blazed" hologram, having grooves with a sawtooth profile.[18] The phase effect of this profile can be represented as $\varphi = s \cdot Mod(\alpha, 2\pi)$ where s is a scaling constant and the function Mod(m, n) is the remainder on division of m by n. For example, in the case of a flat hologram, $\alpha = 2\pi \frac{x}{p}$, where p is the period of the grating while in the case of pitchfork hologram $\alpha = 2\pi \frac{x}{p} + \ell\theta$. In both cases, p is assumed constant. For s = 1, the profile ensures a 100% efficiency as the whole intensity is concentrated in a single diffracted beam.[17]

The aim of this paper is to show that, instead of the so-far adopted amplitude holograms, phase holograms characterized by higher diffraction efficiency can be obtained by FIB nanofabrication of a Si_3N_4 membrane.

In order to predict and account for the experimental intensity of each diffracted beam as a function of the real phase profile produced by FIB milling, we use both a complete numerical treatment of the propagation in the Fresnel regime and an analytical treatment of the diffraction gratings in the Fraunhofer regime. The theory is based on the plane-wave spectral representation of the wave field transmitted by the grating, of periodicity p, reported, for example, in Goodman textbook[19] and gives us a simple expression for the complex amplitude of the m-order diffracted beam, A_m, as a function of the physical parameters included in the phase modulation. A_m, in turn, determine the diffraction efficiency η_m (here the incoming intensity I_m is normalized to 1)

$$A_m = \frac{1}{p}\int_0^p T_H(x)e^{-im\alpha}dx, \tag{3}$$

$$\eta_m = |A_m|^2. \tag{4}$$

For a pure phase grating and using Eq. (2), the transmittance (1) can then be expressed by

$$T_H(x) = e^{iC_E V_{mip} t(x)}, \tag{5}$$

here *t(x)* is the 1-D thickness profile of the hologram and V_{mip} is the mean inner potential of the Si_3N_4 membrane. For simplicity, we consider here the case of a plain grating, although the vortex term would not alter the final result. The amplitude of the m-th diffracted beam is then expressed by

$$A_m = \frac{1}{p}\int_0^p e^{-i\left(C_E V_{mip} t(x) - 2\pi m\frac{x}{p}\right)}dx. \tag{6}$$

It is easy to infer that, if the thickness varies linearly with x and an appropriate coefficient is introduced (as in a tuned blazed profile), only a single component A_m is different from 0. In a real case, the thickness profile can be considered as the piecewise linear model where the combination of the linear sections produce different A_m contributions. We will exploit this approximation to calculate the m-th amplitude values for the different thickness profiles measured in the holograms.

Nanofabrication of the holograms was performed with a Dual-Beam instrument (FEI Strata DB235M), combining a Ga-ion FIB and a scanning electron microscope (SEM), by FIB-milling the silicon-nitride membranes. The nominally 200 nm-thick membranes (217 nm measured) were coated with a 120 nm-thick Au film in order to stop electron transmission except from the patterned areas. This procedure ensures that the intensity in the transmitted beam arises only from the hologram region.

The FIB magnification was adjusted in order to have a 150 nm width and 300 nm periodicity for the grooves composing the hologram, resulting in a full hologram size of 5 × 5 μm^2. The holograms were patterned in two stages: first, the Au layer was uniformly removed over a 5 μm circle area, and then the hologram pattern was superimposed to the exposed region and milled into the silicon nitride.

Figure 1(a) reports a typical SEM image of the FIB nanofabricated hologram and Figure 1(b) shows a typical thickness map, obtained by energy filtered electron microscopy. The measured thickness is 120 nm and 183 nm at the bottom and top of the grooves, respectively; this latter value is in good agreement with the direct measurement of 185 nm obtained from SEM images.

The edge dislocation responsible for the existence of the phase singularity in the diffracted beam is clearly visible. The average thickness profile (Figure 1(c)), resembles a smoothed sawtooth profile. For comparison, an ideal sawtooth or "blazed" profile is also represented in Figure 1(d).

TABLE I. Efficiencies for different types of amplitude and phase hologram. For the case of phase hologram, the optimal phase jump for each is assumed.[17]

	Amplitude hologram		Phase hologram	
Grating profile	Diffraction orders	$\eta_{\pm 1}^{max}$ (%)	Diffraction orders	$\eta_{\pm 1}^{max}$ (%)
Sinusoidal	0, ±1	6.25	All	33.85
Squared	Odd	10.13	Odd	40.52
Blazed	All	2.53	First order	100

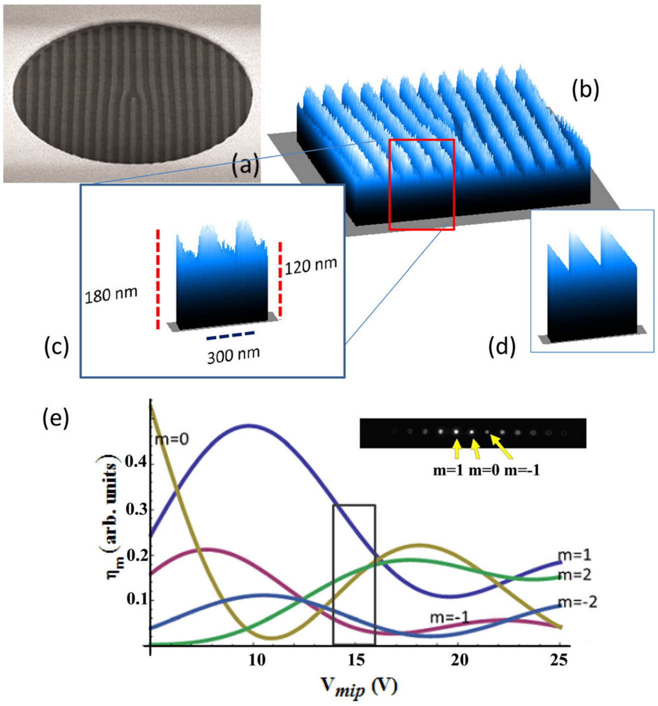

FIG. 1. (a) SEM image and (b) thickness map of the FIB fabricated holographic phase plate (side view) (b). The map has been numerically obtained from the ratio between the elastic image, obtained by putting an energy window of 5 eV around the zero loss peak and the unfiltered image. (c) Thickness profile extracted from (b). (d) Thickness profile for an ideal "blazed" hologram. (e) Diffraction efficiency for different order of diffraction (a diffraction pattern is represented in the inset) as a function of the value of the mean inner potential V_{mip}. The gray box identifies a range of values of mean inner potentials compatible with the experimental diffraction efficiencies.

In order to apply the analytical model of Eq. (6), the single groove profile in Fig 1(c) has been fitted by a stepwise profile

$$t(x) = \begin{cases} a_1 x + b_1 & X_0 < x \le X_1 \\ a_2 x + b_2 & X_1 < x \le X_2 \\ a_3 x + b_3 & X_2 < x \le X_3 \\ a_4 x + b_4 & X_3 < x \le X_4, \end{cases} \tag{7}$$

where the a_j and b_j are the linear interpolation parameters valid in the intervals $[X_j, X_{j+1}]$.

Moreover, for a single groove, $X_0 = 0$ and $X_4 = p$. In this approximation, the diffracted amplitude can be expressed as

$$A_m = -i\sum_{j=1}^{4} e^{iC_E V_{mip} b_j}\Big[\Big(e^{i\left(C_E V_{mip} a_j - \frac{2\pi m}{p}\right)X_j} - e^{i\left(C_E V_{mip} a_j - \frac{2\pi m}{p}\right)X_{j-1}}\Big)/(C_E V_{mip} a_j p - 2\pi m)\Big] \tag{8}$$

from which the diffraction efficiencies for each diffracted beam can be calculated using Eq. (4).

In Figure 1(e), the diffraction efficiencies are plotted according to (8) for $m = 0, 1, -1, 2, -2$ as a function of V_{mip}. For increasing V_{mip}, the destructive interference induces a reduction of the transmitted beam and the simultaneous rise of the $m = 1$ beam up to a maximum obtained for $V_{mip} = 10$ V. Beyond such tuning value, the $m = 1$ drops in intensity mainly in favor of the $m = 2$ beam.

The holographic plate has been inserted into the microscope at the usual specimen position to act as a diffraction grating. The vortex beams have been produced and imaged using a JEOL 2200Fx operated at 200 keV equipped with a Schottky field emitter and an in-column Ω-filter.[16]

The experiments have been performed using the "Low Magnification mode" where the main objective lens has been turned off: this allows for a longer focal length in the further lenses. A systematic variation of the other lenses (in particular the Objective minilens) permitted us to move from an image plane to the Fresnel and Fraunhofer diffraction regions. This special mode allows us to obtain a diffraction angle aperture around 1 μrad. In Figure 2, a series of micrographs from the images plane (conjugated to the holographic plate) to the Fraunhofer plane are shown as a function of the propagation distance Z. The images clearly display three important characteristics:

(i) The beam $m = 1$ is more intense than the transmitted beam. This can be explained recalling the previous theory as a tuning effect of the phase hologram. In this particular case, we obtained an efficiency of ∼25% that is higher than the best obtained with amplitude holograms (see Table I).

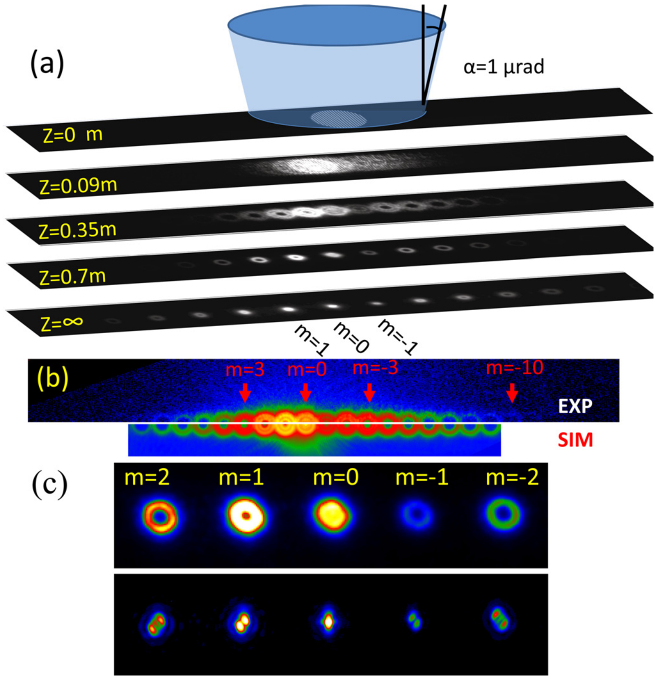

FIG. 2. (a) Experimental through-focus series from the image plane of the hologram to the Fraunhofer plane, showing the evolution of diffracted beams by a hologram with topological charge $\ell = 1$. The hologram is illuminated by a convergent beam with convergence α that produces a partially coherent diffraction. The propagation distance Z is also indicated on the side. (b) Comparison between the experiments for $Z = 0.35$ m (up) and the simulations (down). Both simulated and experimental intensities are represented in logarithmic color-scale. The best fit of the experimental features is obtained for $\alpha = 1$ μrad and a mean inner potential of $V_{mip} = 14$ V. The red line marks the position of the central, undiffracted beam characterized by $m = 0$ and of a few selected diffracted beams. (c) Fraunhofer diffraction pattern in stigmatic (up) and astigmatic (down) conditions. The deliberate introduction of condenser astigmatism induces the transformation between Laguerre-Gaussian to Hermite-Gaussian mode. This permits the easy identification of the transmitted beam that shows a single lobe. The beam with the higher intensity is the beam $m = 1$.

(ii) The intensity distribution is strongly asymmetric. This is a typical effect because of the groove profile asymmetry that violates the parity of the hologram and therefore of the diffraction.

(iii) High order up to the 10th is clearly visible (see also Fig. 2(b)). This is a side benefit of the strong suppression of the transmitted beam and of the complex shape of the profile that can be fitted with many linear pieces of many different slopes, including a steep slope on the left (in Fig. 1(c)) side of the profile.

It is therefore interesting to notice that high values of orbital angular momentum could be reached in this way, if the order of the singularity ℓ of the fork hologram was also raised.

The experimental characteristics described above have been compared with the analytical model. The value of V_{mip} which gives the best agreement with all experimental diffracted intensities is marked by the gray rectangle of Fig. 2. In this region, the m = 1 beam is indeed more intense than the transmitted one and all the other beams are in the expected proportions. The best estimation for V_{mip} is 15 V, in reasonable agreement with the literature value[20] of 16.7 V, measured in thin polycrystalline films of silicon nitride with the same nominal stoichiometry.

We also performed a full numerical simulation of the Fresnel diffraction starting from the exact thickness profile as measured by the energy loss map in Fig. 1 and considering the convolution with an appropriate Fresnel propagator in the parabolic approximation.[21]

To this aim, a specific routine has been implemented inside the STEM_CELL[22] software. The software permits us also to generalize to the case of a tilted or convergent illumination of the hologram.[21] This latter can be considered as a superposition of the results for the different illuminations in the illumination cone.

An example of a simulated pattern is plotted in Figure 2(b) tiled to the experimental image for a propagation distance of 0.35 m and a convergence angle of 1 μrad. The best agreement was obtained assuming a mean inner potential of $V_{mip} = 14 \pm 1$ V, which is in reasonable agreement with the literature value and the analytical evaluation.

Since the difference in the intensity and shape of the different diffracted beams are small, it can be still questioned the experimental assignment of the $m = 0$ beam. Therefore, we also performed an additional experiment deliberately introducing some condenser astigmatism before the hologram. As predicted by Schattschneider *et al.*,[23] the astigmatism produces a conversion of the circular mode approximately described as Laguerre Gaussian to Hermite Gaussian. The order of the diffraction for these modes is equal to the number of lobes clearly visible in the center. The result is visible in Figure 2(c). This allows us to directly assign the transmitted mode and to confirm that the $m = 1$ mode is more intense than $m = 0$.

In conclusion, we have demonstrated experimentally the first holographic phase plate for the generation of orbital angular momentum state in an electron beam.

We have shown that an efficiency as high as 25% can be obtained on a single diffracted beam, thanks to a smoothed sawtooth shape of the profile that is reasonably close to the optimal design for a phase hologram. The full propagation in Fresnel and Fraunhofer mode of such beams has been followed by accurate TEM imaging in "low-mag" mode and found in agreement with numerical simulations and an analytical model.

The data demonstrate that an accurate control of the groove profile can be used to further raise the diffraction efficiency[26] on a single diffracted beam or to generate high quanta of orbital angular momentum.

This is expected to be a breakthrough innovation for all applications of OAM beams and most noticeably for nanoscale circular dichroism measurements that requires a high signal-to-noise ratio and the excitation of a single OAM mode.[3,8,24,25]

E.K. and R.W.B. acknowledge the support of the Canada Excellence Research Chairs (CERC) Program. E.M acknowledges the support of SPINNER 2013. During the final resubmission, we became aware of an extended abstract on phase hologram.[26]

[1] K. Y. Bliokh, Y. P. Bliokh, S. Savel'ev, and F. Nori, Phys. Rev. Lett. **99**, 190404 (2007).
[2] M. Uchida and A. Tonomura, Nature **464**, 737 (2010).
[3] J. Verbeeck, H. Tian, and P. Schattschneider, Nature **467**, 301 (2010).
[4] B. J. McMorran, A. Agrawal, I. M. Anderson, A. A. Herzing, H. J. Lezec, J. J. McClelland, and J. Unguris, Science **331**, 192 (2011).
[5] K. Y. Bliokh, M. R. Dennis, and F. Nori, Phys. Rev Lett. **107**, 174802 (2011).
[6] P. Schattschneider and J. Verbeeck, Ultramicroscopy **111**, 1461–1468 (2011).
[7] A. Jesacher, S. Furhapter, S. Bernet, and M. Ritsch-Marte, Phys. Rev. Lett. **94**, 233902 (2005).
[8] P. Schattschneider, B. Schaffer, I. Ennen, and J. Verbeeck, Phys. Rev. B **85**, 134422 (2012).
[9] J. Verbeeck, P. Schattschneider, S. Lazar, M. Stöger-Pollach, S. Löffles, A. Steiger-Thirsfeld, and G. Van Tendeloo, Appl. Phys. Lett. **99**, 203109 (2011).
[10] J. Verbeeck, H. Tian, and G. Van Tendeloo, Adv. Mater. **25**, 1114–1117 (2013).
[11] E. Karimi, L. Marucci, V. Grillo, and E. Santamato, Phys. Rev. Lett. **108**, 044801 (2012).
[12] L. Clark, A. Béché, G. Guzzinati, A. Lubk, M. Mazilu, R. Van Boxem, and J. Verbeeck, Phys. Rev. Lett. **111**, 064801 (2013).
[13] E. Bolduc, N. Bent, E. Santamato, E. Karimi, and R. W. Boyd, Opt. Lett. **38**, 3546 (2013).
[14] V. Y. Bazhenov, M. V. Vasnetsov, and M. S. Soskin, JETP Lett. **52**, 429 (1990).
[15] N. R. Heckenberg, R. McDuff, C. P. Smith, H. Rubinsztein-Dunlop, and M. J. Wegener, Opt. Quantum Electron. **24**, S951 (1992).
[16] H. Reimer and H. Kohl, *Transmission Electron Microscopy*, 3rd ed., Springer Series in Optical Sciences, Vol 36 (Springer-Verlag, New York, 1993).
[17] E. Karimi, "Generation and manipulation of laser beams carrying orbital angular momentum for classical and quantum information applications," Ph.D. dissertation (Università degli studi di Napoli "Federico II", 2009), see http://www.fedoa.unina.it/3784/.
[18] H. Lichte, Cryst. Res. Technol. **35**, 887 (2000).
[19] J. W. Goodman, *Introduction to Fourier Optics*, 2nd ed. (McGraw International Editions, 1996), Chap.3.
[20] S. Bhattacharyya, C. T. Koch, and M. Rühle, Ultramicroscopy **106**, 525 (2006).
[21] E. J. Kirkland, *Advanced Computing in Electron Microscopy* (Springer, Berlin, 2010).
[22] V. Grillo and E. Rotunno, Ultramicroscopy **125**, 97 (2013).
[23] P. Schattschneider, M. Stöger-Pollach, and J. Verbeeck, Phys. Rev. Lett. **109**, 084801 (2012).
[24] P. Schattschneider, S. Löffler, M. Stöger-Pollach, and J. Verbeeck, Ultramicroscopy **136**, 81–85 (2014).
[25] J. Rusz and S. Bhowmick, Phys. Rev. Lett. **111**, 105504 (2013).
[26] J. S. Pierce, T. R. Harvey, T. S. Yahn, and B. J. McMorran, Microsc. Microanal. **19**, 1188–1189 (2013).